FATIGUE RELIABILITY ASSESSMENT OF WELDED JOINTS OF VERY FAST FERRY ACCOUNTING FOR VEHICLE LOADS

(DOI No: 10.3940/rina.ijme.2011.a4.214)

Y Garbatov & C Guedes Soares, Instituto Superior Técnico, Technical University of Lisbon, Portugal

SUMMARY

This work deals with the fatigue reliability assessment of a welded joint in a longitudinal stiffener of trapezoidal shape in a very fast ferry. Based on the analysis of wave and cargo induced loads the ship hull structure is evaluated. The local structure is represented by a longitudinal stiffener with a trapezoidal transverse section. The critical hot-spots and the stress distributions are defined by FEM. The fatigue damage assessment of considered hot spots is analysed accounting for the combination of wave induced and car-breaking transient loadings. The formulation for the assessment of the welded steel joint is based on the S-N approach and FORM/SORM techniques are applied to evaluate the reliability against fatigue failure accounting for corrosion deterioration. The structural system composed by several hot spots is evaluated as a series system based on second order reliability bounds.

1. INTRODUCTION

Fast ferries are high-speed ships, capable of carrying both cars and passengers at a minimum speed of 25 knots. Increased speed has drastically reduced journey time, greatly improving passenger comfort level. High service speeds of these vessels are possible due to their specific lightweight hull constructions and structural design. By adopting higher strength steel, instead of the traditional mild steel, the structures can be subjected to higher loads, resulting from either more extreme operational conditions or from lighter thin plated structures, [1].

This paper addresses the fatigue reliability assessment of welded joints of a fast ferry's car deck for trucks with very high tensile steel trapezoidal stiffeners. Special trapezoidal shaped longitudinals are designed as vehicle deck stiffeners.

Two different welding connections, between trapezoid longitudinals and deck plate, are examined: spot-weld and all-weld connections. The spot-weld connection refers to welding of the stiffeners using a spot-weld technique of welding of several points with appropriate spacing while the all-weld connection refers to classical, continuous welding along the longitudinal length.

The finite element analysis is performed on two levels: global and detailed local analysis. The global finite element model of the mid ship part of the very fast ferry is subjected to two different loading conditions, one for the ship in hogging and another one for the ship in sagging. In both cases additional design pressure loads are applied on the corresponding decks. The structural detail of concern is located at the middle of the span between two transverse frames, where the longitudinal trapezoidal stiffener is connected by backing strip plate. Detailed finite element analysis was performed to obtain critical hot spot stresses and overall stress distribution. More details were reported by Garbatov et al. [2].

The stiffener is considered to be supported by the transverse frames, and loaded axially by the vertical hull girder bending moment and by additional transverse force due to the presence of truck-breaking load. The hot spots are analyzed accounting for the combination of transversal and axial loads. As a result of the performed analysis, stress concentration factors are defined and subsequently used for fatigue damage and reliability calculation taking into account the combination of low frequency wave induced loads and transient vehicle loads, accounting also for corrosion deterioration with time.

This fatigue damage assessment is accomplished by several steps of calculation. The considered fatigue loading comprises wave and a truck breaking load effect, which has been already used by Garbatov et al. [3] when performing a fatigue analysis of the joint. Here a detailed reliability analysis of fatigue damage will be presented.

Fatigue damage assessment of this kind of welded joints is based on the hot spot stress approach, being one of the most practical methods in combination with detailed finite element analysis as has been demonstrated by Fricke and Petershagen [4], Niemi [5] and Niemi et al. [6].

However, Xiao and Yamada [7] proposed a method for evaluating the structural stress approach based on the stress at a location 1 [mm] below the weld toe surface in the direction corresponding to the expected crack path, where the finite element analysis uses a mesh size having an element size of 1 mm or less.

The effective notch stress approach was proposed by Radaj [8]. Further research about this approach has been conducted by Radaj et al. [9] and the effective notch stress approach has been included in the IIW fatigue design recommendations, with the fatigue strength design curve of FAT 225 for welded steel joints.

It has to be pointed out that the calculated local stress, around the structural singularities, depends very much on the structural idealization, the element type used and the mesh subdivision.

Marine structures operate in a complex environment, which is defined by water properties such as salinity, temperature, oxygen content, pH level and chemical composition that can vary and influence the corrosion deterioration.

The effect of the different factors on the behaviour of corrosion have been analysed by Guedes Soares, et al. [10] in marine atmosphere and for immersion corrosion by Guedes Soares, et al. [11] all over the ship's service life.

Reliability based methods have gained acceptance as being proper tools to support design decisions and for assessing the level of safety in structures. The inspection and repair work performed during the ship lifetime never allows a very dramatic spreading of cracks to be developed and this effect was incorporated in the time variant formulation of ship hull reliability by Guedes Soares and Garbatov [12]. That formulation and the corresponding results yield the required information to assess the effect of inspections and repairs at different points in time on the reliability of the hull girder.

A similar formulation can be made for the effect of corrosion on ship reliability as shown by Guedes Soares and Garbatov [13], but normally both fatigue and corrosion are present and their combined effect needs to be considered in that the decrease net section due to corrosion will increase the stress levels, which in turn increase fatigue damage. This effect has been recognised by Guedes Soares and Garbatov[14].

Fatigue damage of structural joints accounting for nonlinear corrosion has been analysed by Garbatov, et al. [15] and fatigue reliability of maintained welded joints in the side shell of tankers by Garbatov and Guedes Soares [16].

The study presented here covers a complete stochastic fatigue damage analysis of a 25 year service life for a very fast ferry. The fatigue analysis of the vessel is conducted in a way that environment, operational conditions and structural are taken into account. The ferry is expected to operate in a zone with particular sea-state conditions.

The assessment of fatigue damage of welded steel joints is based on the S-N approach and thus this assessment accounts for the whole ship lifetime and is time independent.

The effect of corrosion deterioration leads to a decrease of plate thickness with time and a consequent increase of the stress levels and thus of the fatigue damage predicted by the S-N approach. FORM/SORM techniques are then applied to evaluate the reliability of structural joints against fatigue failure. It must be noted however that this approach is different from the one of Guedes Soares and Garbatov [12] in which fatigue damage was calculated by the crack growth model of Paris Erdogan.

2. FINITE ELEMENT MODELING

The global finite element model of the ferry was generated containing all longitudinal elements that contribute to the longitudinal strength. All existing longitudinals are introduced in the model using beam finite elements. The length of the fast-ferry global model in longitudinal, i.e. x-axis, direction is 36 meters and comparing to the ship breadth of 24.70m is being considered to be sufficient in size for global deformation analysis.

The deck No 5 of the fast ferry was designed for trucks that are supposed to be driven in, parked and driven out. Trucks are loaded with heavy cargo. The fast ferry is carrying cars and trucks parked on several decks. The main particulars of the ferry analysed here are length, L=205.00 m, breadth, B=24.70 m, depth, D=9.00 m, draught, T=5.42 m, draught, speed, v=50.00 kn, light ship weight, LW=6932.13 t and deadweight, DW=2769.87 t.

To properly take into account both global and local loads, two-step sub model finite element analysis is performed based on Guedes Soares, et al. [17].

The mid ship part of the ferry that forms the global finite element model was generated using 2-node beam and 3-node and 4-node shell elements. The global model finite element mesh is presented in Figure 1.

The global model consists of 10,034 2-node beam elements, 9,802 4-node shell elements and 6,626 3-node shell elements. It has a total of 74,640 degrees of freedom.

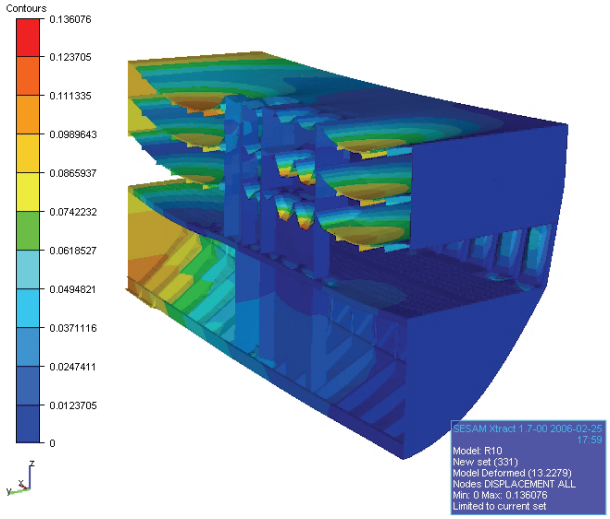

Figure 1- Global model deformation, sagging

Boundary conditions are defined in a way that the aft side cross-section is fixed in all degrees of freedom, while the fore side cross-section is rigid, so that sections may remain in plane after the load is applied (sectional moments). In this way symmetry of the load and boundary conditions is satisfied.

The loading applied to the global model consists of sectional design moments, transverse pressure loads on decks and water induced pressure load on the hull for both hogging and sagging loading condition.

The supporting (or backing-reinforcement) strip plate connects the two longitudinals - it is bent so that it fits precisely under the longitudinal and serves as a support during welding. The supporting plate is 40mm wide and the weld root gap between longitudinals is 5 mm wide. During the welding process a supporting plate is welded to the longitudinal and acts as its reinforcement. The trapezoidal longitudinal reinforcement is entirely connected to the deck plate by spot welds.

Spot welds along the trapezoidal longitudinal are 20 mm wide and distanced 80 mm from each other. Alternatively, continuous welding is used and the longitudinal is continuously connected to the deck plate.

The distance between transverse frames is equal to the length of the sub-model, 2,400 mm. The two neighbouring transverse frames represent the boundaries of the sub-model. The minimum width of the sub-model is 700 mm, which corresponds to transverse distance between trapezoidal longitudinals. The sub-model height is 158 mm (see Fig. 2 to 4).

The two local models, spot-weld and all-weld model, are generated using volume finite elements (20-node solid and 15-node solid) so that the weld geometry may be taken properly into account (see Figure 2 and Figure 3). The local model, or sub-model, consists of 9,502 finite elements 19,466 nodes and 58,398 degrees of freedom.

Near the supporting plate, i.e. at the middle of the longitudinal span, the neighbouring finite element width varies from 4mm to 7.5mm wide. In this way, it does not conform strictly with the usual "txtxt" requirement of the hotspot stress evaluation procedure, where t is the thickness of the plating. Finite element width variation was made during precise modelling of support plate and surrounding welds and geometry.

The all-weld model has the same finite element mesh size as the spot-weld model, except the weld geometry.

The loading of the local model consists of prescribed displacements from the global model, both in hogging and sagging loading conditions, and a concentrated force of 48.75 kN (car-breaking load) acting at the middle of the local model span. It is considered that breaking load is acting only during the boarding.

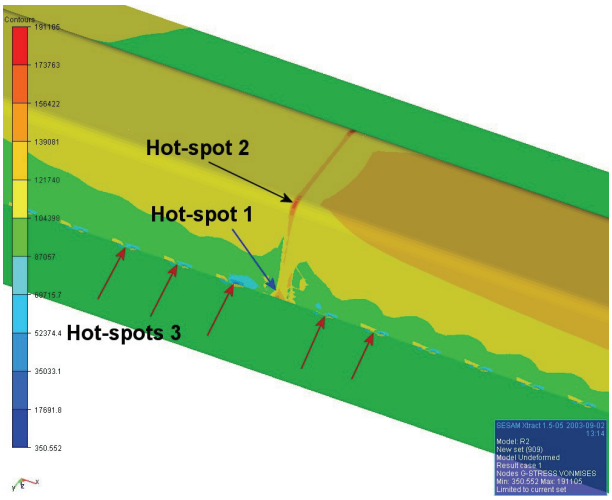

Figure 2 – Hot spot 1 to 3 for spot-weld model

The concentrated force represents a truck tire load that is acting at the middle of the longitudinal span. Concentrated forces are acting on four neighbouring spot welds. The truck tire contact surface is relatively small and if the model force acts directly to the deck plate it would produce very large stresses.

The spot-weld model stress distribution is shown in Figure 2, where three types of highly stressed areas may be distinguished (hotspots 1, 2 and 3).

Three areas of high stress concentration (Hotspot 4, 5 and 6) may be observed for the all-weld finite element model, Figure 3. The hot spot 4 on the all-weld model corresponds to the hotspot 2 of the spot-weld model.

The hot spot 6 in the all-weld model corresponds to the hotspot 3 in the spot-weld model and it is presented with red arrow in Figure 3. High stress is affecting both the deck plate and the trapezoid longitudinal, so the weld toe becomes a subject for the hot spot stress evaluation.

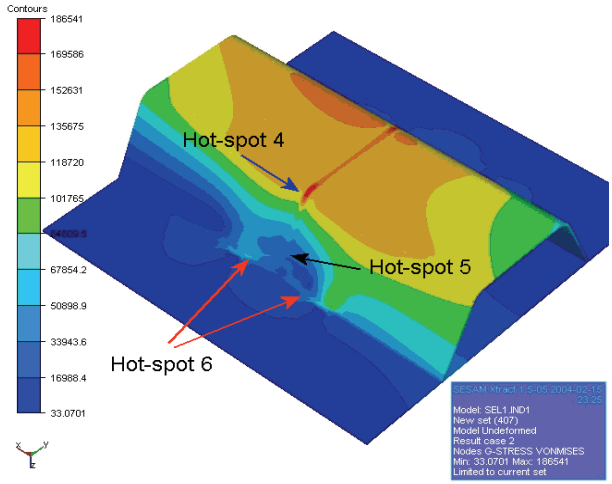

Figure 3 – Hot spots 4 to 6 for all-weld model

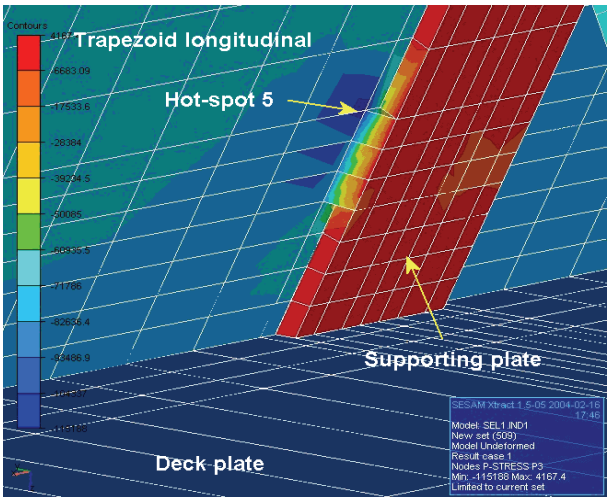

Figure 4 – Hot spots 5

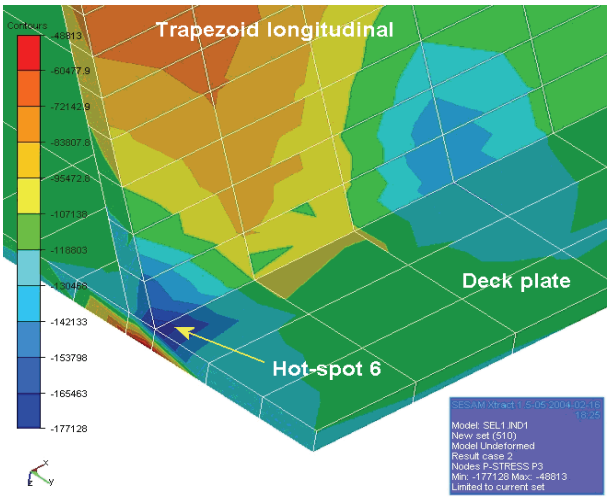

Figure 5 – Hot spot 6, all-weld model

The hot spot 5 is shown in Figure 4. The high stress concentration is located at the edge of the small side weld that connects the supporting plate with the trapezoid longitudinal. Figure 5 presents the hot spot 6 in detail.

3. HOTSPOT STRESS ANALYSIS

The aim of the hotspot stress analysis is to evaluate the stresses at the structural detail weld toe. The International Institute of Welding [6] presented the extrapolation procedure following advances in research on that topic and gives recommendation on how to effectively apply for the hotspot extrapolation procedure.

The hot spot principal stresses are determined by direct computation using finite element analysis. The mesh refinement of the local finite element model is sufficient and with element lengths near high stress zones equal to the plate thickness. A linear extrapolation is employed in hot spot stress calculations.

As 20-node solid finite elements are used, nodal stresses were available directly from the solver results. The direction of the principal stresses was examined with the aim of stress vector presentation.

The stress concentration factor, SCF is commonly defined as the ratio of the hot-spot stress, $\sigma_{hot-spot}$ and the normal stress, σ_n i.e.:

$$SCF = \frac{\sigma_{hot\ spot}}{\sigma_n} \qquad (1)$$

The stress concentration factor measures the increase of stress concentration in a particular spot and is used for fatigue life estimation based on S-N curve approach.

The stress concentration factor at the hot spot 1 is 1.73 and at the hot spot 2 is 1.67. The stress concentration factor at the hot spot 3 location has rather high value for the hogging loading condition and for the local load case 2 i.e. SCF=2.69. This is the highest stress concentration factor concerning all the cases.

The stress concentration factor at the hot spot 4 location is 1.89. This may be compared directly to the stress concentration factor of 1.67 for the hot spot 2, as this is the same spot on both spot-weld and all-weld models. The SCF for the 5th and 6th location are 1.32 and 1.48 respectively.

4. FATIGUE DAMAGE

The trapezoid longitudinal of concern is located below the car deck and it is subjected to both lateral and axial load. The lateral load is provoked by the truck breaking load and has the magnitude of 48.75 kN for the vehicle under consideration. The truck breaking load is induced due to the breaking of car on the position of parking on the deck.

It is considered that the wave induced stresses in the welded joints studied may be described as a Gaussian process with zero mean value. In that case the stress amplitude distribution follows the Rayleigh distribution for any short sea state. The long-term stress distribution is defined based on Rayleigh short sea-state induced stress distributions and are quantified as a function of the probability of occurrence of any sea state of reference. The probability density function for the sea state conditions may differ and different distributions may be adjusted.

The linear model assumption is generally adequate, but in severe seas, the response may not be linear and a nonlinear analysis should be conducted.

The combination of wave induced load with the loads due to cargo operation (low and high frequency loads) is applied in this work. It is observed that the duration of the impulse force in the case of the cargo operation is rather small.

It is considered as a linear elasto-dynamic problem, which means that the damping coefficient is proportional to the velocity of displacement and the recovering to the initial state force is a linear function.

The excitation amplitude of nominal stresses at the point of study is as a function of the axial load subjected to the structures due to the vertical induced bending moment. Vertical bending moment at a probability level of 10^{-8}, representing 25 years lifespan with an operating time at sea is defined by direct calculations. The vertical bending moment acting for a life time of 0.85*25=21.25 years at sea close to a midship section is with an absolute value of 680 MNm.

The wave-induced stresses $\sigma_w(t)$ are considered as a stationary, narrow-banded Gaussian process with a zero mean and variance, σ_{σ_w} are described as:

$$\sigma_w(t) = \sigma_{a_w} cos(\omega_w t + \varepsilon_w) , \quad (2)$$

where σ_{a_w} is the normal stress amplitude, ω_w is the natural frequency for the first elastic mode of vibration and ε_w is the phase angle. For the case studied here ω_w is assumed as 0.93 radian per second and ε_w is considered 0. The amplitude σ_{a_w} is a random variable, which for a short sea-state condition may follow a Rayleigh distribution.

The car breaking load applied to the stiffener is treated as a transient process:

$$\sigma_c(t) = \sigma_{a_c} exp(-k_c \omega_c t) sin(\omega_c t + \varepsilon_c) \quad (3)$$

where σ_{a_c} is the excitation normal stress amplitude, ω_c is the natural frequency assumed as 3.64 radian per second, k_c =0.04 is damping factor and ε_c is the phase angle.

The excitation amplitude, σ_{a_c} of the transient process, $\sigma_c(t)$, is considered as a random variable that follows a Rayleigh distribution which implies that the process can be treated as a narrow-band Gaussian process with time-dependent variance. The combination of $\sigma_w(t)$ and $\sigma_c(t)$ then becomes the sum of a stationary Gaussian process and a transient one. The process is similar to that of the combination of two stationary processes, but has differences.

The car breaking loading induces stresses that result in additional damage to the wave induced load damage and this is modelled as a transient process. For simplification here, the phase angles are not taken into account.

The fatigue damage assessment is based on the Miner [18] summation rule. The basic assumption of the method is that the structural damage per load cycle is constant at a given stress range. It is assumed that the stress range is distributed according to a two-parameter Weibull distribution and fatigue damage for wave-induced load is calculated using the close form solution of Nolte and Hansford [19] as:

$$D_w = \frac{v_o T_d}{K} \frac{\Delta\sigma_w^m}{\left[Ln(n_o)\right]^{m/\alpha}} \Gamma\left(1+\frac{m}{\alpha}\right) \quad (4)$$

and the fatigue damage for the transient process is calculated as proposed by Jiao and Moan [20] as:

$$D_c = \frac{n_o \left(2\sqrt{2}\right)^m \Gamma\left(1+\frac{m}{2}\right) \Delta\sigma_c^m}{2K\left[Ln(n_c)\right]^{m/2}\left[1-exp(-2\pi km)\right]} , \quad (5)$$

where the material descriptors of the S-N curve are taken from [21] as $K = 10^{12.38}$, m=3 and v_o =0.11 and α =1. The number of car breaking cases during a service life, considered in the example here, is 1622. The stress range, $\Delta\sigma_i$ is calculated as:

$$\Delta\sigma_{i,n} = \left(\sigma_{i,a,tensile} - \sigma_{i,a,compressive}\right) \quad (6)$$

$$\Delta\sigma_i = SCF_i \ \Delta\sigma_{i,n} \quad (7)$$

where SCF_i is the stress concentration factor of the hotspot considered. Finally the total fatigue damage for any hotspot is calculated as:

$$D = D_w + D_c \quad (8)$$

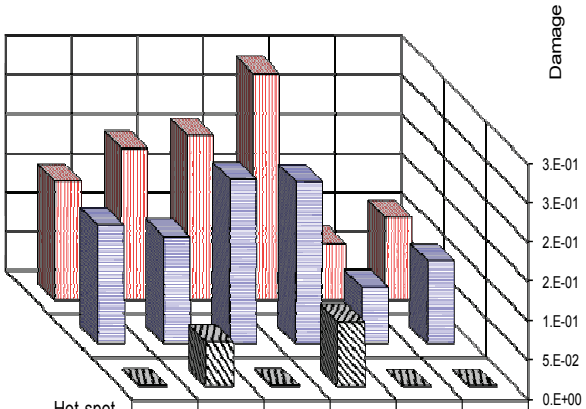

Hot-spot	1	2	3	4	5	6
Car breaking	9.52E-04	5.71E-02	1.29E-03	8.28E-02	1.20E-05	5.96E-04
Wave	1.51E-01	1.36E-01	2.09E-01	2.06E-01	7.23E-02	1.05E-01
Total	1.52E-01	1.93E-01	2.10E-01	2.89E-01	7.23E-02	1.06E-01

Figure 6– Fatigue damage of Hotspots 1 to 6

The fatigue analysis of the welded joint reveals six areas of high stress concentration. The fatigue damage for the spot-weld model as hotspot 1, 2 and 3 respectively and

for the all-weld model is denoted as hotspot 4, 5 and 6 respectively. The fatigue damage of the welded joint due to the contribution of different loading is shown in Figure 6.
It can be seen from Figure 6 that in general, fatigue damage is lower for the all-weld model than the spot-weld model. The location of highest fatigue damage for the all-weld longitudinal and for the spot-weld longitudinal is the hotspot 4.

5. GENERAL CORROSION

Corrosion of interior spaces in ship structures has an important role in the long-term structural integrity. Under conditions of high temperature, inappropriate ventilation, high stress concentration, high stress cycling, high rates of corrosion can be achieved at specific structural details such as horizontal stringers or longitudinal and web frames.

The conventional models for general corrosion wastage presented for example by Guedes Soares [22] assumed a constant corrosion rate, leading to a linear relationship between the corrosion thickness and time. Experimental evidence of corrosion, reported by various authors, shows that a non-linear model is more appropriate.

Guedes Soares and Garbatov, [23, 24] proposed a model for the non-linear time-dependent function of general corrosion wastage. This time-dependent model separates corrosion degradation into three phases. In the first one there is no corrosion because the protection of the metal surface works properly. The second phase is initiated when the corrosion protection is damaged and corresponds to the start of corrosion, which decreases the thickness of the plate. The third phase corresponds to a stop in the corrosion process and the corrosion rate becomes zero.

The model used to define the corrosion deterioration here is based on the solution of a differential equation of the corrosion wastage proposed by Guedes Soares and Garbatov [24]:

$$d(t)=\begin{cases} d_{\infty}\left(1-e^{-\frac{t-\tau_c}{\tau_t}}\right), & t\geq\tau_c \\ 0, & t<\tau_c \end{cases} \tag{9}$$

where d_{∞} is the long-term corrosion wastage (d_{∞} is less or equal of as a build thickness), $d(t)$ is the corrosion wastage at time t, τ_c is the time without corrosion which corresponds to the start of failure of the corrosion protection coating (when there is one), τ_t is the transition time (see Figure 7).

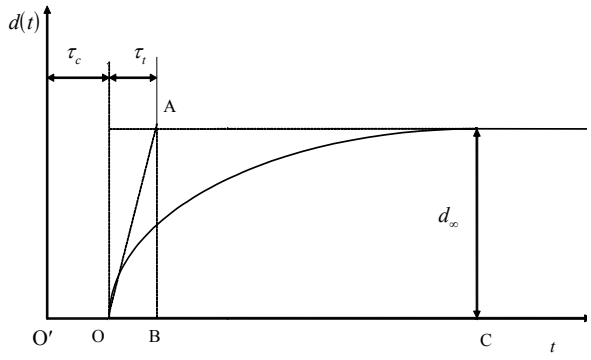

Figure 7 Thickness of corrosion wastage, [23, 24]

This model has been validated and calibrated with corroded plate data from tankers, allowing representative values of the parameters to be determined [25].

The long-term wastage is defined as an extreme value in the service time interval for deck. The descriptors of the regression equation of the corrosion depth for the long-term corrosion wastage for truck deck plates is d_{∞}=2.3 mm. The coating life for deck plates is τ_c=3 years and the transition period of deck plates is τ_t=17.24 years are assumed here.

6. RELIABILITY ASSESSMENT

The reliability analysis presented here is using FORM/SORM techniques to identify a set of basic random variables, which influence the failure mode or the limit-state under consideration. The limit-state function is formulated in terms of the *n* basic variables given as:

$$g(X)=g(X_1,X_2,...,X_n) \tag{10}$$

This function defines a failure surface when equals to 0. It defines an (*n*-1) dimensional surface in the space of n basic variables. This surface divides the basic variable space into a safe region, where $g(x)>0$ and an unsafe region where $g(x)<0$. The failure probability of a structural component with respect to a single failure mode can formally be written as:

$$P_f=P\left[g(x)\leq 0\right]=\int_{g(x)\leq 0} f_X(x)\,dx \tag{11}$$

where $f_X(.)$ is the joint probability density function of the *n* basic variables and P_f denotes probability of failure. The *n*-dimensional integral is defined over the failure region.

In practical applications, the reliability cannot be evaluated in the exact manner as given by Eqn 11. This is

because enough statistical data is usually not available to develop the *n*-dimensional joint density function of the basic variables. Secondly, even when the joint density function is available, analytical or numerical integration is possible only for a few simple cases. The FORM/SORM methods provide a way of evaluating the reliability efficiently with reasonably good accuracy, which is adequate for practical applications as proposed by Hassofer and Lind [26], Rackwitz and Fiessler [27] and Ditlevsen [28].

Using a FORM/SORM technique and the S-N fatigue damage approach, the limit state equation for fatigue failure may be defined on the basis of Eqns 4, 5 and 9 for $t > \tau_C$, as:

$$g_i\left(\mathbf{X}|t\right) = x_1 - \frac{\left(x_2^{p_1} p_{3,i}^{p_1} p_4 + x_5^{p_1} p_{6,i}^{p_1} p_5\right) p_7^{p_1}}{x_3 p_2 \left\{p_7 - x_4 p_8 \left[1 - \exp\left(-\frac{t - p_9}{p_{10}}\right)\right]\right\}^{p_1}}, \; t > \tau_C \tag{12}$$

where x_i are uncertainties on calculation and p_i are parameters defined in Table 1.

For the hot-spot locations, $i \in [1,6]$ the load characteristics $p_{3i} = q_{wi}$ and $p_{6i} = q_{ci}$ are 12.511, 12.102, 13.956, 13.888, 9.796, 11.101 and 49.166, 192.470, 54.423, 217.825, 11.427, 42.061 MPa respectively.

A Normal distributed random variable B_w was considered to take into account the uncertainty on fatigue stress estimation accounting for the wave-induced loading. As the stress calculation has several steps, each of which with its own uncertainty, the stochastic variable B_w can be split into four components: $B_{L,w}$ modelling the uncertainty in the load calculation, B_σ modelling the uncertainty on the normal stress calculation, B_H modelling the uncertainty of the hot spot stress concentration factors and B_Q modelling the uncertainty on the weld quality and on misalignment. In the same way the uncertainty B_c can be also defined.

The reliability calculations can also be performed using the total uncertainty on fatigue stress estimation represented by the random variable $\tilde{B}$ with mean value and coefficient of variation determined by:

$$\tilde{B} = \prod_i B_i \text{ and } COV(\tilde{B}) = \sqrt{\prod_i \left(1 + C_i^2\right) - 1} \tag{13}$$

The stochastic model of the basic variables considered in this study is presented in Table 2.

The global annual reliability index β is obtained from the probability of failure as:

$$\beta = \Phi^{-1}(P_f) \tag{14}$$

where Φ^{-1} is the standard normal probability distribution function.

Table 1 Parameter descriptions

Variable	Units	
$p_1 = m$	[-]	3.0
$p_2 = K$	[-]	2.4E12
$p_4 = T_d \Gamma\left(1 + \frac{m}{\alpha}\right)$	[Cycle]	4.42E8
$p_5 = \frac{\left(2\sqrt{2}\right)^m \Gamma\left(1 + \frac{m}{2}\right)}{2\left[1 - exp\left(-2\pi km\right)\right]}$	[-]	28.4
$p_7 = h_{deck}$	[m]	0.007
$p_8 = d_\infty$	[m]	0.0023
$p_9 = \tau_C$	[year]	3.0
$p_{10} = \tau_t$	[year]	17.24

Table 2 Stochastic model

Variable	Distribution	Mean Value	St. Dev.
$B_\Delta = x_1$	Log-Normal	1.0	0.2
$B_{L,w}$	Normal	0.85	0.255
B_s	Normal	1.00	0.12
B_H	Normal	1.00	0.30
B_Q	Normal	1.00	0.20
$B_w = x_2$	Normal	0.85	0.48
$B_K = x_3$	Log-Normal	0.8	0.1
$B_{cor} = x_4$	Log-Normal	1.0	0.32
$B_{L,c}$	Normal	0.9	0.15
$B_c = x_5$	Normal	0.9	0.42

Figure 8 presents the results of the fatigue reliability assessment of the six hot spots of the very fast ferry operating during 25 years and accounting for the total damage including wave and car-breaking loadings. Figure 9 is the reliability beta index as a function of time only accounting for wave induced load. The total reliability index, composed by wave and car breaking load, presents severe condition as already was indicated by the results of fatigue damage assessment.

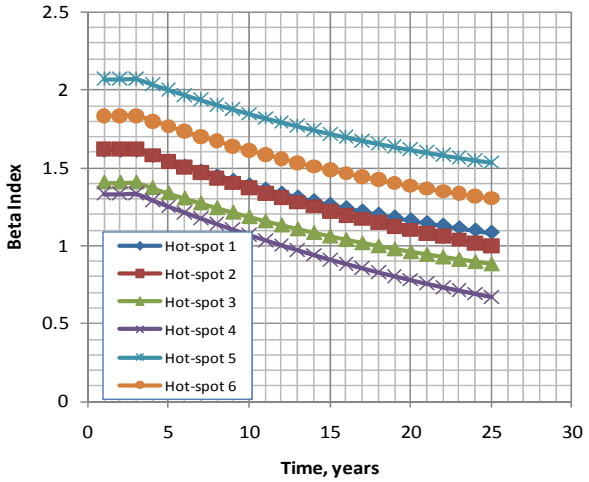

Figure 8 – Beta reliability index, total damage

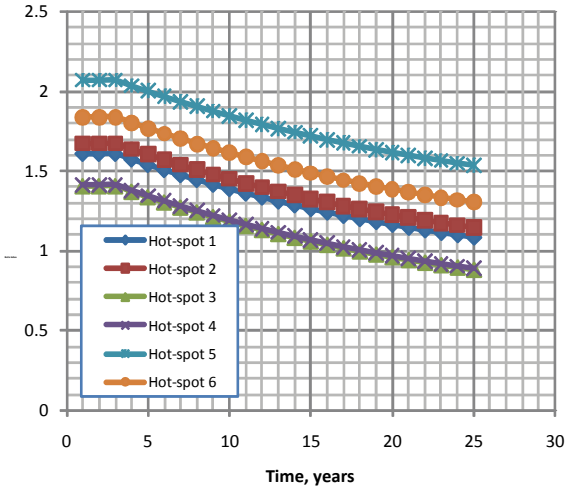

Figure 9 – Beta reliability index, only wave induced damage

The importance of the contribution of each variable to the uncertainty of the limit state function $g(x)$ can be assessed by the sensitivity factors which are determined by:

$$\alpha_i = -\frac{1}{\sqrt{\sum_{i=1}^{\infty}\left(\frac{\partial g(\underline{x})}{\partial x_i}\right)^2}}\frac{\partial g(\underline{x})}{\partial x_i} \qquad (15)$$

Figure 10 shows the sensitivities of the failure function with respect to changes in the variables for the hot-spot 4 in the case of full-welded joint. A positive sensitivity indicates that an increase in a variable results in an increase in the failure function and positively contributes to reliability.

It can be seen from Figure 10 that the importance of the uncertainty on fatigue damage and on the scale parameter of the Weibull distribution of stress range are almost identical and the overall uncertainty on fatigue stress estimation is quite important on the results especially the uncertainty on load calculation, which together with the uncertainties rising from corrosion deterioration are by far the most important variables. It has to be pointed out the effect of corrosion determination has only to be accounted after the coating is finished.

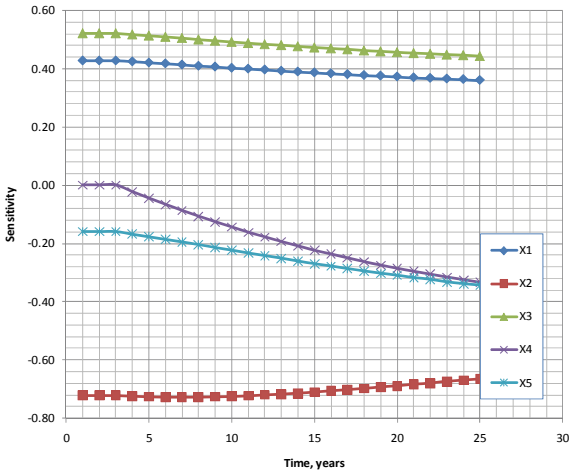

Figure 10 – Sensitivities of the variables, Hot-spot 4

The probability of failure of any of the structural hot-spot is defined by:

$$P_{f,i}(t) = 1 - \Phi\left[\beta_i(t)\right] \qquad (16)$$

where $P_{f,i}(t)$ is the probability of failure and β_i is the reliability index.

Considering the probability of failure of a series system of three hot-spots, each of which is modelled with a safety margin:

$$M_i = g_i(\mathbf{X}),\ i \in [1,3] \qquad (17)$$

The FORM probability of failure for ith hot-spot can be given as:

$$P_{f_i} = P(M_i \le 0) = P(g_i(\mathbf{X}) \le 0) \approx P(\beta_i - \alpha_i^T U \le 0) = \Phi(-\beta_i) \qquad (18)$$

The series system fails if just one of the hot-spots fails, which may be defined as:

$$P_f^s = P\left(\bigcup_{i=1}^{m} M_i \le 0\right) = 1 - \Phi_m(\boldsymbol{\beta};\boldsymbol{\rho}) \qquad (19)$$

where Φ_m is the m-dimensional normal distribution function. It has been used that the correlation coefficient ρ_{ij} between two linearized safety margins $M_i = \beta_i - \alpha_i^T U$ and $M_j = \beta_j - \alpha_j^T U$ is $\rho_{ij} = \alpha_i^T \alpha_j$.

A formal generalised series system reliability index is given as:

$$\beta^s = -\Phi^{-1}\left(P_f^s\right). \tag{20}$$

To evaluate the series system the second order Ditlevsen [29] bounds are used here:

$$\Phi\left(-\beta^s\right) \le \sum_{i=1}^{m}\Phi\left(-\beta_i\right) - \sum_{i=2}^{m} max\left\{\Phi\left(-\beta_i\right) + \sum_{j=1}^{i-1}\Phi_2\left(-\beta_i,-\beta_j;\rho_{ij}\right),0\right\} \tag{21}$$

$$\Phi\left(-\beta^s\right) \le \sum_{i=1}^{m}\Phi\left(-\beta_i\right) - \sum_{i=2}^{m} max\left\{\Phi_2\left(-\beta_i,-\beta_j;\rho_{ij}\right)\right\} \tag{22}$$

The numbering of the failure elements influences the bounds. A good choice to arrange the failure elements is to account them to degreasing probability of failure.

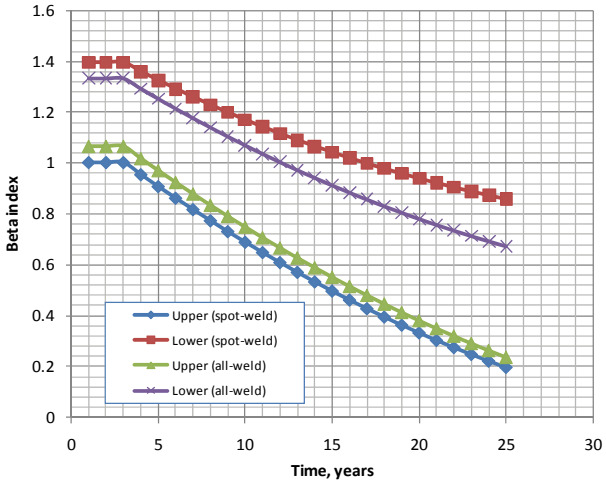

Figure 11 – Beta index, series system- second order bounds

Two series system are composed. The first one is related to the spot-weld structure including the hot-spots 1, 2 and 3 and the second one is for the hot-spots 4, 5 and 6 of the all-welded structure. The correlation coefficient of the probability of failure, due to the very close location of the hot-spots and similarity in the loading conditions, are assumed here as very high and equal to 0.99.

As can be seen from Figure 11, the lower bound of the all-weld structure demonstrates lower reliability in comparison to the spot-weld one. This is explained with the fact that the lower bound is related to a series system where the system components are 100 % correlated and the weakest element will dominate the system reliability. In the study here the hot-spot 4, which is a part of the all-weld structure, has the lowest reliability index.

The upper bound of the spot-weld structure is lower than the one for the all-weld structure.

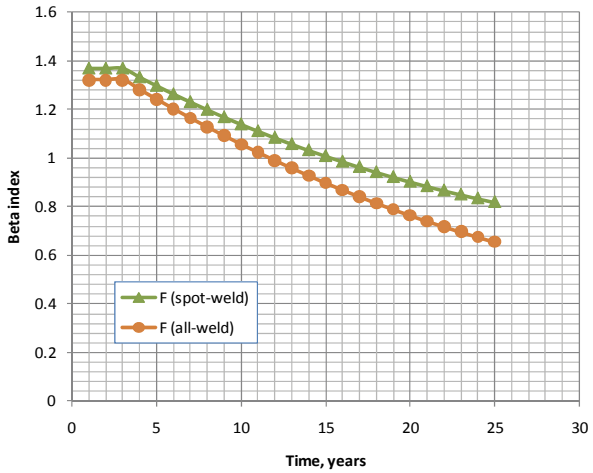

Figure 12 – Beta index, series system

Eqns (21) and (22) presented a bound and it is convenient to calculate a specific value. Feng [30] developed a point estimate for the joint probability of failure as:

$$P_{f,ij} = \left[P_{f,i} + P_{f,j}\right]\left[1 - arccos\left(\rho_{ij}\right)/\pi\right] \tag{23}$$

Eqn (23) has high accuracy to be used in Eqn (21) and (22).

The final result for the system reliability of spot-weld and all-weld structure is given in Figure 12. As may be observed the spot-weld joint has a better reliably performance during the service life of 25 years without accounting for the repair and maintenance actions.

7. CONCLUSIONS

The work presented here analyzed the fatigue reliability of ship hull structural joints accounting for wave induced loads as well as vehicle operational loads. Different welding connections between trapezoid longitudinals and deck plate were examined. A set of case studies were analyzed taking into account global loading conditions, including two local finite element models performing spot-weld and all-weld analysis.

Analysis of the all-weld model revealed three areas of high stress concentration, one of them being the same as on the spot-weld model. The location of highest fatigue damage for the all-weld longitudinal and for the spot-weld longitudinal is the bending of the trapezoid.

As a result of the performed analysis the beta reliability indexes are defined based on the combination of low frequency wave induced loads and transient loads accounting for the corrosion deterioration.

The structure modelled as a series system composed by hot-spot elements was evaluated based on the second order bounds. The all-welded structure demonstrated a

low beta index bounds for the low bound in comparison to the spot-welded one. It is explained with the fact that the reliability of the weakest element dominates the lower bound, which in this particular case is the hot-spot 4.

9. REFERENCES

1. JANSSEN, G. T. M., Fatigue Based Design Rules for the Application of High Tensile Steel in Ships, *Proceedings of the Seventh International Marine Design Conference*, pp. 317-328, 2000.
2. GARBATOV, Y., RUDAN, S. AND GUEDES SOARES, C., Fatigue Assessment of Welded Trapezoidal Joints of Very Fast Ferry Subjected to Combined Load, *Engineering Structures*, 32, pp. 800-807, 2010.
3. GARBATOV, Y., SANTOS, J. M. AND GUEDES SOARES, C., Effect of Truck Induced Load on Welded Structural Joints Subjected to Fatigue. In: *Maritime Transportation and Exploitation of Ocean and Coastal Resources*, Vol. 1, C. Guedes Soares, Y. Garbatov and N. Fonseca, editors, London, UK: Taylor & Francis Group, pp. 387-394, 2005.
4. FRICKE, W. AND PETERSHAGEN, H., Detail Design of Welded Ship Structures Based on Hot-Spot Stresses, *Proceedings of the Practical Design of Ships and Mobile Units*, J. B. Caldwell and G. Ward, Elsevier Science Limited, Vol. 2, pp. 1087-1100, 1992.
5. NIEMI, E. E., *Recommendation Concerning Stress Determination for Fatigue Analysis of Weld Components*: Abington Publishing, 1995.
6. Niemi, E., Fricke, W. and Maddox, S., Structural Stress Approach to Fatigue Analysis of Welded Components - Designer´s Guide. In: IIW Doc. XIII-1819-00/XV-1090-01, 2004.
7. XIAO, Z.-G. AND YAMADA, K., A Method of Determining Geometric Stress for Fatigue Strength Evaluation of Steel Welded Joints, *International Journal of Fatigue*, 26, pp. 1277-1285, 2004.
8. RADAJ, D., *Design and Analysis of Fatigue-Resistant Welded Structures*, Cambridge: Abington Publishing, 1990.
9. RADAJ, D., SONSINO, C. M. AND FRICKE, W., Recent developments in local concepts of fatigue assessment of welded joints, *International Journal of Fatigue*, 31, (1), pp. 2-11, 2009.
10. GUEDES SOARES, C., GARBATOV, Y., ZAYED, A. AND WANG, G., Influence of Environmental Factors on Corrosion of Ship Structures in Marine Atmosphere, *Corrosion Science*, 51, (9), pp. 2014-2026, 2009.
11. GUEDES SOARES, C., GARBATOV, Y., ZAYED, A. AND WANG, G., Corrosion Wastage Model for Ship Crude Oil Tanks, *Corrosion Science*, 50, (11), pp. 3095-3106, 2008.
12. GUEDES SOARES, C. AND GARBATOV, Y., Fatigue Reliability of the Ship Hull Girder, *Marine Structures*, 9, pp. 495-516, 1996.
13. GUEDES SOARES, C. AND GARBATOV, Y., Reliability of Maintained Ship Hulls Subjected to Corrosion, *Journal of Ship Research*, 40, pp. 235-243, 1996.
14. GUEDES SOARES, C. AND GARBATOV, Y., Reliability of Maintained Ship Hull Subjected to Corrosion and Fatigue, *Structural Safety*, 20, pp. 201-219, 1998.
15. GARBATOV, Y., RUDAN, S. AND GUEDES SOARES, C., Fatigue Damage of Structural Joints Accounting for Non-linear Corrosion, *Journal of Ship Research*, 46, pp. 289-298, 2002.
16. GARBATOV, Y. AND GUEDES SOARES, C., Fatigue Reliability of Maintained Welded Joints in the Side Shell of Tankers, *Journal of Offshore Mechanics and Arctic Engineering*, 120, pp. 2-9, 1998.
17. GUEDES SOARES, C., GARBATOV, Y. AND VON SELLE, H., Ftigue Damage Assessment of Ship Structural Components Based on the Long-term Distribution of Local Stresses, *International Shipbuilding Progress*, 50, pp. 35-56, 2003.
18. MINER, M., Cumulative Damage in Fatigue, *Journal of Applied Mechanics*, 3, pp. 159-163, 1945.
19. NOLTE, K. AND HANSFORD, J., Closed-form expressions for determining the fatigue damage of structures due to ocean waves, *Proceedings Offshore Technology Conference*, pp. 861-870, 1976.
20. JIAO, G. AND MOAN, T., Reliability-Based Fatigue and Fracture Design Criteria for Welded Offshore Structure, *Engineering Fracture Mechanics*, 41, pp. 271-282, 1992.
21. DNV, *Fatigue Assessment of Ship Structures, Classification Notes No 30.7*, 1998.
22. GUEDES SOARES, C., Ship Structural Reliability, *Risk and Reliability in Marine Technology*, pp. 227-245, 1988.
23. GUEDES SOARES, C. AND GARBATOV, Y., Non-linear Time Dependent Model of Corrosion for the Reliability Assessment of Maintained Structural Components. In: *Safety and Reliability*, Vol. 2, S. Lydersen, G. K. Hansen and H. A. Sandtov, editors, Rotterdam, The Netherlands: A. A. Balkema, pp. 928-936, 1998.
24. GUEDES SOARES, C. AND GARBATOV, Y., Reliability of Maintained, Corrosion Protected Plates Subjected to Non-Linear Corrosion and Compressive Loads, *Marine Structures*, pp. 425-445, 1999.
25. GARBATOV, Y., GUEDES SOARES, C. AND WANG, G., Non-linear Time Dependent Corrosion Wastage of Deck Plates of Ballast and Cargo Tanks of Tankers, *Journal of*

Offshore Mechanics and Arctic Engineering, 129, pp. 48-55, 2007.

26. HASOFER, A. M. AND LIND, N. C., An Exact and Invariant First-Order Reliability Format, *Journal of Engineering Mechanics Division*, 100, pp. 111-121, 1974.
27. RACKWITZ, R. AND FIESSLER, B., Structural Reliability Under Combined Random Load Sequences, *Computers and Structures*, Vol. 9, pp. 489-494, 1978.
28. DITLEVSEN, O., Generalised Second Moment Reliability Index, *Journal of Structural Mechanics*, 7, pp. 435-451, 1979.
29. DITLEVSEN, O., Narrow Reliability Bounds for Structural Systems, *Journal of Structural Mechanics*, 7, pp. 453-472, 1979.
30. FENG, Y. S., A method for computing structural system reliability with high accuracy, *Computer & Structures*, 33, (1), pp. 1-5, 1989.

